Photoinduced Electron Transfer and Geminate Recombination in Solution

L. Song,† S. F. Swallen, R. C. Dorfman,‡ K. Weidemaier, and M. D. Fayer*
Department of Chemistry, Stanford University, Stanford, California 94305
Received: July 16, 1992; In Final Form: November 13, 1992

Intermolecular electron transfer and geminate recombination are explored experimentally in both solid and liquid solutions using the same donor–acceptor pair. The solvents were chosen to have similar chemical and dielectric properties, but vastly different viscosities. Systems of an electron donor, rubrene, and varying concentrations of an electron acceptor, duroquinone, were studied. The solvents used were diethyl sebacate (liquid) and sucrose octaacetate (solid). Forward electron transfer was studied using time-resolved and steady-state fluorescence measurements for a variety of acceptor concentrations. Electron back-transfer (geminate recombination) was measured using pump–probe experiments. The data were analyzed using a theoretical treatment that takes into account diffusion of the donor and acceptors, a distance-dependent (exponential) transfer rate, Coulomb interactions between the ions generated by the forward transfer, and donor–acceptor and acceptor–acceptor excluded volumes. The forward transfer data, in both the solid and liquid solutions, are in very good agreement with calculations. Virtually identical forward transfer parameters are obtained from the solid and liquid samples. The back-transfer parameters obtained from the measurements on solid solution are able to reproduce the liquid solution's back-transfer data, but only when the high-frequency dielectric constant is used. The use of this value for the dielectric constant is discussed.

I. Introduction

Photoinduced electron transfer from a donor molecule to an acceptor molecule is responsible for an important class of chemical reactions. Following the photoinduced transfer of an electron from a neutral donor to a neutral acceptor, the highly reactive radical ions that are created can go on to do useful chemistry.[1-3] In this paper, an experimental study is presented on the influence of molecular diffusion on photoinduced electron transfer and geminate recombination. Steady-state fluorescence yield and time-resolved fluorescence measurements were used to determine the population of the donor's excited state, and pump–probe experiments were used to measure the population of ion pairs produced as a result of electron transfer. Since electron transfer quenches the fluorescence from the excited state, fluorescence provides a direct observable for the yield and time dependence of the forward electron-transfer process. The pump–probe observable is proportional to the population that is not in the ground state of the system. The pump–probe measurement examines the two higher energy states of the donor–acceptor system: the excited state and the reactive state (the ion pair produced by forward electron transfer). The time-dependent reactive state population is determined by combining the results of the pump–probe and time-resolved fluorescence experiments.

Photoinduced electron transfer between randomly distributed donors and acceptors embedded in solid solution has been studied theoretically[1,5-7] and experimentally.[1,8] Recently, diffusion-influenced electron transfer has also been treated theoretically[4,9-12] and experimentally.[10,13] Molecular diffusion has a complex effect on the state populations for the forward and back transfer processes. The experiments presented here examine the time evolution of the state populations. The results are compared to a recently developed theory.

An important aspect of this work is that the experiments were performed in both solid and liquid solutions on the same donor–acceptor pair. In solid solution, there is no molecular diffusion on the time scale of the experiment; thus, the viscosity is considered to be infinite. The data are analyzed using a method which includes a distance-dependent rate of electron transfer,[4,5] and accounts for a random distribution of acceptors about a donor. In liquid solution, the theory must also include the effects due to molecular motion. The state populations are analyzed taking into account the additional effects of diffusion and the Coulomb interaction between ions.[4,5] The solid solution is described by the liquid solution problem in the limit where the diffusion constant is equal to zero. For each solution, both the excited-state and reactive-state populations are obtained using a method that includes donor–acceptor and acceptor–acceptor excluded volumes, and donor–acceptor reflecting boundary conditions.[4] The solid and liquid solvents were chosen to have very similar dielectric properties. Therefore, within the context of the theoretical model, the only difference between the solid and liquid is the rate of diffusion.

The purpose of this paper is to examine the statistical mechanics of the problem of photoinduced electron transfer and geminate recombination in liquid solution. The standard quantum mechanical model for the distance-dependent electron-transfer rate between a donor–acceptor pair (neutrals or ions) is assumed. The transfer rate falls off exponentially with distance.[13,28] In a system of donors and acceptors that are initially randomly distributed and are undergoing diffusive motion, properly performing the spatial averages over all possible configurations is complex. Theoretical solutions to this problem have been presented previously.[29-33] However, the complexity of the problem is greatly magnified when geminate recombination is included. The distribution of spatial separations of ion pairs formed by forward electron transfer is not random. Rather, it is determined by the details of the forward transfer dynamics. In addition, the motions of the ions are not diffusive because of the attractive Coulomb interaction between the oppositely charged ions. The distribution of initial pair separations is highly skewed to short distance, and thus, even for moderately high dielectric constants, the Coulomb attraction has a profound effect.[4]

The comparison between solid and liquid solutions provides an important control for judging the applicability of the statistical mechanics theoretical treatment. For a solid solution (fixed donor and acceptor positions), the necessary spatial averages can be calculated exactly.[38,39] The forward and back electron-transfer parameters for the solid solution are obtained from

† Present address: Department of Chemistry and Biochemistry, University of California at Los Angeles, Los Angeles, CA 90024.
‡ Present address: Chemistry Department, University of Texas at Austin, Austin, TX 78712.

0022-3654/93/2097-1374$04.00/0

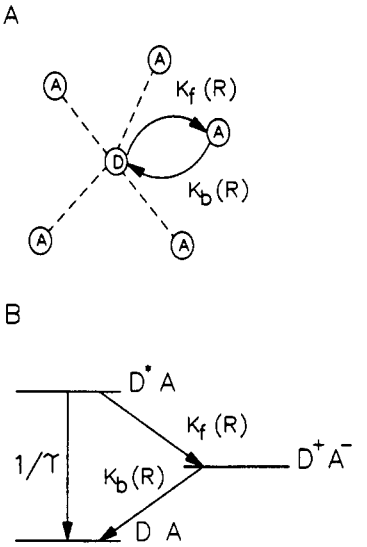

Figure 1. (A) A diagrammatic representation of forward and back (geminate) electron transfer. This model depicts the situation studied here, i.e., an excited donor surrounded by a higher concentration of neutral acceptors. (B) A level diagram showing the three states, the ground (DA), excited (D^*A), and reactive (D^+A^-) states. The three rate processes are represented by their rates, τ, $k_f(R)$, and $k_b(R)$, which are the fluorescence lifetime of the donor and the forward and back transfer rates, respectively.

measurements of samples with varying acceptor concentrations. Then, in principle, experimental results from liquid solution can be analyzed using the same transfer parameters and the theory that now includes diffusion. In the experiments presented below, the forward transfer data obtained from time-resolved and steady-state fluorescence closely agree with the theory. The forward transfer parameters obtained from liquid solution are virtually identical to those found in solid solution. The back-transfer dynamics in solid solution, obtained from pump–probe experiments as a function of acceptor concentration, show very good agreement with theory. When the solid solution back-transfer parameters are used in the liquid solution theory, very good agreement with experiment is again found if the high-frequency dielectric constant is used. The use of the low-frequency dielectric constant results in very poor agreement between theory and experiment, no matter how the back-transfer parameters are varied. This result is unexpected, and is discussed qualitatively in terms of the distance scales involved in the electron-transfer dynamics.

II. Theoretical Approach

In this section, a brief description of the theoretical approach used to analyze the data is presented. The equations necessary for fitting the experimental data are given. Complete details of the theory have been presented previously.[4,5]

In the model, the donors and acceptors are randomly distributed at $t = 0$ when the sample is excited. The donor has only one accessible electronic excited state, and the acceptor has only one higher energy state as a radical anion. After pulsed excitation, two processes can occur from the excited state: electron transfer or decay to the ground state by fluorescence or radiationless relaxation. The forward and back electron-transfer rates are exponentially decaying functions of distance.[13,28] The electron donor rubrene is reported to have essentially unit quantum yield for fluorescence.[14] The unquenched fluorescence decay of rubrene is exponential.

Electron transfer from the excited state generates a positive radical ion and a negative radical ion. This ion pair is referred to as the reactive state (see Figure 1). After forward electron transfer, back electron transfer can occur, returning the system to the ground state with neutral donor and acceptor. The rate constants for excited-state decay (k), forward electron transfer (k_f), and electron back-transfer (k_b) are

$$k = 1/\tau \tag{1}$$

$$k_f(R_0) = \frac{1}{\tau}\exp\left(\frac{R_f - R_0}{a_f}\right) \tag{2}$$

$$k_b(R_0) = \frac{1}{\tau}\exp\left(\frac{R_b - R_0}{a_b}\right) \tag{3}$$

where R_0 is the donor–acceptor initial separation. (In solid solution the separation remains fixed, but in liquids it evolves over time.) R_f, a_f, R_b, and a_b are molecular parameters that characterize the distance scale of the forward (f) and backward (b) transfer rates. τ is the donor excited-state lifetime in the absence of acceptors. In eqs 2 and 3, τ is used to characterize the time scale of the electron-transfer process. The choice of the time scale is arbitrary and does not influence the results. While τ is not inherently related to the forward or back electron transfer, it is the natural choice since the excited-state lifetime is an intrinsic time scale in the problem. Electron transfer from a radical anion to a neutral acceptor (self-exchange) is not included in the model. In systems of quinones such as the acceptor (duroquinone) used here, the self-exchange rate is quite slow[40] on the time scale of the electron-transfer dynamics observed in these experiments.

There are two steps involved in calculating the excited-state and reactive-state populations. The first is deriving the survival probabilities for the excited (ex) and reactive (re) states for a single donor–acceptor pair as a function of initial separation.[9-12] The second step is to use the survival probabilities in the ensemble-averaged equations for state populations. These calculations are performed in the thermodynamic limit.[4,9-12]

In solid solution, the survival probabilities are given by[4]

$$S_{ex}(t|R_0) = \exp(-k_f(R_0)t) \tag{4}$$

$$S_{re}(t|R_0) = \exp(-k_b(R_0)t) \tag{5}$$

where R_0 is the donor–acceptor separation at $t = 0$. In solid solution the donor–acceptor separation does not change with time. In liquid solution, the following equations are used to obtain the survival probabilities:[4,10,15]

$$(\partial/\partial t)S_{ex}(t|R_0) = D\nabla^2_{R_0}S_{ex}(t|R_0) - k_f(R_0)\,S_{ex}(t|R_0) \tag{6}$$

$$S_{ex}(0|R_0) = 1 \tag{7}$$

$$4\pi R_m{}^2 D(\partial/\partial R_0)S_{ex}(t|R_0)|_{R_0=R_m} = 0 \tag{8}$$

$$(\partial/\partial t)S_{re}(t|R_0) = L^*_{R_0}S_{re}(t|R_0) - k_b(R_0)\,S_{re}(t|R_0) \tag{9}$$

$$S_{re}(0|R_0) = 1 \tag{10}$$

$$4\pi R_m{}^2 D(\partial/\partial R_0)S_{re}(t|R_0)|_{R_0=R_m} = 0 \tag{11}$$

where D is the sum of the donor (D_D) and the acceptor (D_A) diffusion constants and

$$\nabla^2_{R_0} = \frac{2}{R_0}\frac{\partial}{\partial R_0} + \frac{\partial^2}{\partial R_0{}^2} \tag{12}$$

$$L^*_{R_0} = \frac{1}{R_0{}^2}\exp(V(R_0))\,\frac{\partial}{\partial R_0}DR_0{}^2\exp(-V(R_0))\,\frac{\partial}{\partial R_0} \tag{13}$$

$$V(R_0) = \left[\frac{Z_D Z_A e^2}{4\pi\epsilon_0\epsilon_r K_B T}\right]\frac{1}{R_0} \tag{14}$$

The diffusion operators are for the spherically symmetric case, and $V(R_0)$ is the Coulomb potential.

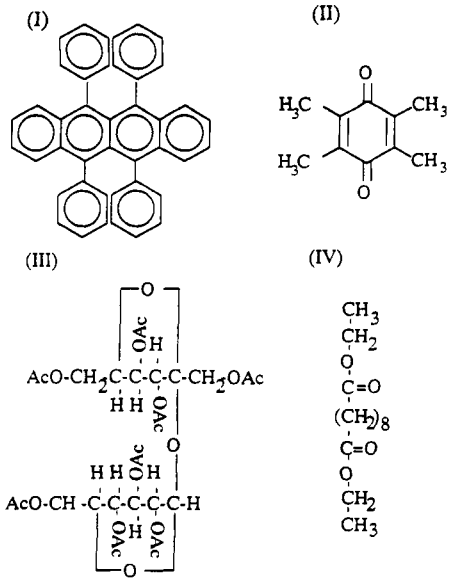

Figure 2. Structures of (I) rubrene (9,10,11,12-tetraphenylnaphthacene), (II) duroquinone (tetramethyl-1,4-benzoquinone), (III) sucrose octaacetate ($C_{28}H_{38}O_{19}$), and (IV) diethyl sebacate ($C_2H_5O_2C(CH_2)_8CO_2C_2H_5$).

The solutions to eqs 6 and 9 give the excited- and reactive-state survival probabilities, respectively. These equations cannot be solved analytically. There are, however, analytical solutions for very small[16] and very large[17] diffusion constants. There are also solutions for transfer only at contact.[10,15] The experiments presented below represent the general case since the diffusion explored in this work is intermediate between the very fast and very slow diffusion limits. An exponentially decaying distance-dependent electron-transfer rate is also included. Equations 7 and 10 are the initial conditions. Equations 8 and 11 are the reflecting boundary conditions. Reflecting boundary conditions are used since the transfer rate is finite even at contact, giving some probability of a donor and acceptor coming together and then diffusing apart without electron transfer occurring.

To obtain the excited-state and reactive-state populations for solid or liquid solution, the appropriate survival probabilities given above are substituted into the equations below:[4,5,18,19]

$$\langle P_{ex}(t)\rangle = \exp(-t/\tau)\exp((4\pi/d^3)\times \int_{R_m}^{\infty} \ln\,[1-p+pS_{ex}(t|R_0)]R_0^2\,dR_0) \quad (15)$$

$$\langle P_{re}(t)\rangle = 4\pi C\int_{R_m}^{\infty}\int_0^t \frac{S_{re}(t-t'|R_0)\langle P_{ex}(t')\rangle}{1-p+pS_{ex}(t'|R_0)}\times \left[-\frac{\partial S_{ex}(t'|R_0)}{\partial t'}\right] dt' R_0^2\,dR_0 \quad (16)$$

where R_m is the sum of the donor and acceptor radii, d is the acceptor diameter, τ is the donor excited-state fluorescence lifetime, $p = Cd^3$, and C is the concentration of acceptors in number density units. Equations 15 and 16 take into account donor–acceptor and acceptor–acceptor excluded volumes. The probability that the system is found in any one of the three states, the ground ($\langle P_{gr}\rangle$), excited ($\langle P_{ex}\rangle$), or reactive ($\langle P_{re}\rangle$) state, is unity. Therefore, the ground-state population is

$$\langle P_{gr}(t)\rangle = 1 - \langle P_{ex}(t)\rangle - \langle P_{re}(t)\rangle \quad (17)$$

III. Experimental Procedures

A. Sample Preparation. The samples are composed of the donor rubrene (RU), and the acceptor duroquinone (DQ), dissolved in either sucrose octaacetate (SOA) or diethyl sebacate (DES). Figure 2 shows the structures of RU, DQ, SOA, and DES. SOA is a glass at room temperature while DES is a liquid. In the presence of light and oxygen, RU in solution will oxidize irreversibly. The presence of dust particles in samples increases the amount of scattered light and noise in the experiments. Concentration inhomogeneities in the samples will lead to inconsistent results. These considerations shaped the sample preparation technique.

For the solid (glassy) SOA solutions, the SOA was twice recrystallized from ethanol. DQ was sublimed twice. A small amount of RU was dissolved in a degassed (with argon) solution of SOA in spectral grade acetone in the dark. This solution was filtered through a 0.2-μm filter into a 1-mm-path-length optical cell. The cell was placed on a vacuum line with a liquid nitrogen trap and backfilled with nitrogen to remove oxygen in the atmosphere above the solution. The pressure in the cell was gradually lowered to $\sim 10^{-6}$ Torr in order to evaporate the acetone. When no more acetone could be detected by eye, the sample was melted with a heat gun to remove any residual acetone. The cell was removed from the vacuum line, and DQ was added to the solution. The cell was placed back on the vacuum line and sealed off under vacuum. The sample was heated above 90 °C, the melting point of SOA, in order to dissolve the DQ. While molten, the sample was shaken. This step was repeated several times to ensure a homogeneous distribution of DQ.

By preparing the samples in the dark and using degassed solutions under vacuum, RU's sensitivity to oxygen was eliminated. Samples of RU in SOA as old as 1 year show no signs of decomposition in either their spectra or their appearance. The optical densities of RU and DQ were independent of sample position, demonstrating the uniformity of the samples' concentrations.

The concentrations of DQ and RU in the solid solutions were determined spectroscopically. The extinction coefficient of DQ in SOA at 430 nm was measured from samples of known concentration. The result is 28.8 M^{-1} cm^{-1}. DQ does not absorb at 528 nm. The peak of the S_0–S_1 RU absorption band occurs at 528 nm. The ratio of the extinction coefficients of RU in SOA at 528 nm versus 430 nm is $\epsilon_{528}/\epsilon_{430} = 5.27$. This result was obtained from the ratio of the optical densities (OD). The extinction coefficient of RU in SOA at 528 nm is 11 600 M^{-1} cm^{-1}. To get the DQ optical density, the RU contribution to the OD at 430 nm was subtracted.

The liquid samples were made using serial dilution to obtain the desired concentrations of RU and DQ. Typically the RU concentration was 10^{-4} M. This eliminated problems with dimer formation, reabsorption, and energy transfer. The presence of dimers can be detected by distortions in the RU absorption spectra as a function of concentration. No distortions were seen. For the low concentration of RU used in these experiments, there is no RU–RU energy transfer and no significant reabsorption. The samples had an optical density of $\sim$0.2 at 532 nm. The DQ concentration ranged from 0 to 0.5 M.

The solvent diethyl sebacate (DES) was passed through a 2-μm filter. Each sample was placed in a 1-mm optical cuvette. The cuvette had an adapter for a vacuum line so the sample could be freeze–pump–thawed (3–5 cycles) to remove oxygen and prevent RU decomposition. The samples were sealed under vacuum. The viscosities of pure DES and DQ/DES solutions were measured with an Ubbelohde viscometer. At the highest concentrations of DQ, the viscosities of the solutions differed from the pure solvent by a small amount. The measured viscosities were used.

B. Fluorescence Yield Measurements. The reduction in the RU fluorescence quantum yield caused by electron transfer was measured as a function of acceptor concentration. A CW pumped acoustooptically mode-locked and Q-switched Nd:YAG laser provided single pulses at a 1.0-kHz repetition rate. These pulses were frequency doubled to 532 nm and had a full width half-maximum (fwhm) $\sim$100 ps. The green single pulses were used

for sample excitation. A sample holder was constructed to ensure that each sample was reproducibly illuminated with the same amount of light and that the same solid angle of fluorescence was collected. The fluorescence was passed through a set of 532 nm cutoff filters to eliminate scattered laser light. The broad-band fluorescence was detected by a phototube and a lock-in amplifier. For each sample, a corresponding yield was measured for another sample that contained only RU and solvent (SOA or DES). Dividing the fluorescence intensities of the RU/DQ/solvent samples by the plain RU/solvent sample after correcting for their small differences in RU OD gave the relative fluorescence yield.

C. Time-Resolved Fluorescence. The time-resolved fluorescence decays of the liquid RU/DQ/DES solutions were measured by time-correlated single photon counting. The laser system and the single photon counting instrument have been described in detail elsewhere.[20] Briefly, the frequency-doubled 532-nm output from a mode-locked YAG laser was used to synchronously pump a cavity-dumped dye laser. The excitation wavelength was 555 nm. The fluorescence was detected in a 60-nm window centered at 590 nm. Scattered light was blocked from entering the detector (a multichannel plate) by a 1-mm antislit placed in the position normally occupied by the center slit of a subtractive double monochromator. The instrument response of the system was 70 ps. The detection polarization was set to the magic angle from the excitation polarization to remove the influence of rotational relaxation of the donor molecules from the time dependence of the fluorescence. The output of the instrument was transferred to a computer for data analysis. Measurements were also made with a 532-nm excitation wavelength. The results at both wavelengths were identical.

Measurements of the fluorescence decay can be influenced by the time-dependent relaxation of the solvent. Particularly in systems with molecules which have large dipole changes upon excitation, a significant spectral shift of the fluorescence spectrum can be observed.[13] Rubrene, however, has almost no permanent dipole and experiences no dipole change upon excitation. In addition, the broad spectral bandwidth of the experimental setup would essentially eliminate solvent relaxation effects on the time dependence of the emission.

Intensity studies were carried out to ensure that no thermal effects were present in the fluorescence decays. The pump power was lowered until the signal strength directly scaled with intensity. At this power, no changes were seen in the decay as the intensity was lowered.

The time-resolved fluorescence decays of the solid RU/DQ/SOA solutions were measured on a different apparatus that was in use before the single photon counting setup became available. The same monochromator and multichannel plate setup were used, and fluorescence was detected at the magic angle. The samples were excited at 532 nm using the Nd:YAG laser described above. The signal from the multichannel plate went to a boxcar averager. The sampling window (200 ps) of the boxcar was positioned in time by a 10-V ramp, giving a time range of 100 ns. The digital output of the boxcar was added to the data from previous shots by computer until an adequate signal-to-noise ratio was obtained. The overall time response of the system (1.2 ns) was measured by observing the excitation pulse. The decays in the solid solutions are considerably slower than in liquid solution (see below), so the 1.2-ns response is adequate. The impulse responses of both time-resolved fluorescence systems were recorded and used for convolution with theoretical calculations to permit accurate comparison to the data.

D. Pump–Probe Experiments. The Nd:YAG laser described above was also used for the pump–probe experiments. For this setup, a single green pulse (532 nm, fwhm = 100 ps) was selected and split into an excitation pulse, a probe, and a reference pulse. The excitation pulse was passed through a half-wave-plate and polarizer before entering the sample. This permits adjustments of the intensity and polarization of the pump beam. This beam is chopped with a mechanical chopper at half the laser repetition rate. The probe pulse passes down a mechanical delay line, through a half-wave-plate and polarizer, and then enters the sample. The probe is set to the magic angle relative to the pump beam. The signal is detected through another polarizer set to the same angle as the probe beam. The spot sizes were 200 and 150 μm for the pump and probe, respectively. The signal is detected by a large area photodiode. The third pulse is also passed through the sample. This reference pulse is detected by an identical photodiode. The outputs of the two photodiodes go into the two inputs of a differential amplifier. The intensities of the probe pulse and the reference pulse are adjusted to null the output of the differential amplifier in the absence of the pump pulse. The output of the differential amplifier is measured by a lock-in amplifier set to detect at the chopping frequency. As in the fluorescence measurements, intensity studies were carried out to exclude any high-intensity artifacts. The intensity of the pump beam was typically $\geq$20 times that of the probe.

IV. Results and Discussion

Forward electron transfer was examined by observing RU (donor) fluorescence yields and fluorescence decays as a function of DQ (acceptor) concentrration. Information on geminate recombination was obtained from the concentration dependence of pump–probe experiments. The data were analyzed using the equations that are briefly outlined in section II. There are three basic issues to address: (1) Can the statistical mechanical model describe the data; i.e., can the shape and concentration dependence be reproduced with a single set of fitting parameters? (2) Is there a consistency between the parameters obtained for the solid and liquid solutions? (3) How do the dynamics in the solid and liquid solutions compare?

There are four unknown experimental parameters: the forward electron-transfer rate parameters, R_f and a_f, and the back electron-transfer parameters, R_b and a_b. The forward parameters are obtained from the fluorescence yield and fluorescence decay observables. These variables are independent of the back-transfer parameters. In the solid solution, it is possible to obtain R_f independently of a_f. In the liquid solution, the two observables make it possible to confirm the fits. Once the forward parameters are found, the two back-transfer parameters are obtained from the pump–probe experiments. The comparison between the solid and liquid results provides a check on the determination of the parameters.

In addition to the electron-transfer parameters, the model requires several other constants. They are the excited-state lifetime of RU (τ) and the two molecular sizes: the radius of the donor (R_D) and the radius of the acceptor (R_A). The contact distance is given by $R_m = R_D + R_A$, and the parameter d is $2R_A$. There are three other parameters. There are the sum of the donor and the acceptor molecular diffusion constants in DES, D, the relative permittivity of DES, ϵ_r, and the concentrations of DQ, C, in the various samples. There are other parameters involved in constructing the observables such as absorption and stimulated emission cross-sections for the RU ground and excited states. These will be discussed further below.

The fluorescence lifetimes of RU in SOA and DES were found to be 15.0 and 14.4 ns, respectively. These numbers fall in the range of values measured by others.[14] At room temperature RU has unit quantum yield for fluorescence.[14,23] Thus, there is no significant triplet formation.

The molecular sizes were obtained from X-ray crystallographic data. The values used for the analysis are R_m = 9 Å and d = 7.2 Å.[21] These were calculated by dividing the volume of the unit cell by the number of molecules per unit cell. This gave the molecular volumes. Space-filling models of the molecules were also constructed, and the molecular volumes agreed with the

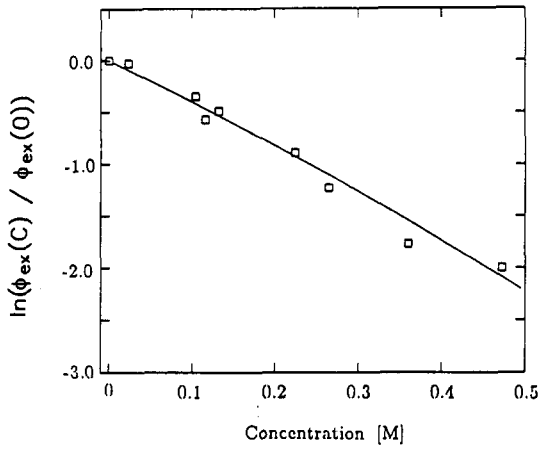

Figure 3. Natural log of the relative fluorescence yield plotted as a function of the acceptor concentration for the solid solution. From this plot one of the two forward transfer parameters for the solid solution is determined. R_f = 13.1 Å.

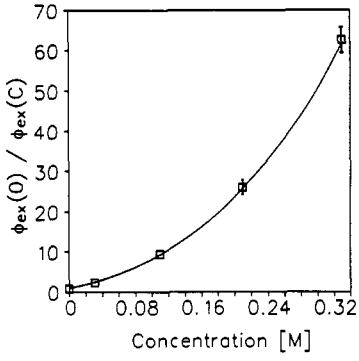

Figure 4. A Stern–Volmer plot of the relative fluorescence yield data for liquid solution. Error bars are shown for two points. The others are smaller than the data squares. The best fit (solid line) gave a_f = 0.22 Å and R_f = 12.8 Å.

numbers obtained using the X-ray crystallographic data. The model takes the molecules to be spheres.

The diffusion constants were obtained by measuring the viscosity of DES and using the Stokes–Einstein equation. The value of D used in the theory is calculated in the donor frame of reference. Thus, the applicable diffusion constant is the sum of the donor and acceptor diffusion constants: $D = D_D + D_A$. The viscosity of DES was measured as a function of DQ concentration. For the concentrations of DQ used here this gave the following diffusion constants: C = 0.031 M, D = 18.3 Å²/ns; C = 0.110 M, D = 18.4 Å²/ns; C = 0.210 M, D = 18.6 Å²/ns; and C = 0.330 M, D = 18.8 Å²/ns. These diffusion constants are consistent with those obtained for similar molecules.[10,14]

The relative permittivity of DES was measured using a capacitance bridge and an air gap capacitor.[22] The measured ϵ_r is 5. The measurement was also performed as a function of DQ concentration, and no variation was found.

A. Fluorescence Yield Measurements. Figures 3 and 4 display the fluorescence yield data and the best fits to the data for the solid and liquid solutions, respectively. For each case the relative yield was calculated using the following equation:

$$\phi_{ex} = (1/\tau) \int_0^\infty \langle P_{ex}(t) \rangle \, dt \qquad (18)$$

The solid solution data are displayed as a Perrin plot.[1,10,14] It is a plot of the natural log of the relative fluorescence yield vs concentration of the acceptor. The data from the liquid solution are displayed as a Stern–Volmer plot.[1,10,14] It is a plot of the inverse fluorescence yield vs concentration of the acceptor. Inokuti and Hirayama[6] found for fixed donor–acceptor positions that the Perrin plot is essentially linear, and its slope is related to the R_f parameter. In the data analysis here, eq 18 was used to fit the data, using eq 15 for the excited-state population. In principle, eq 18 depends on the two forward electron-transfer parameters, R_f and a_f, and the concentration of acceptors, C. However, Inokuti and Hirayama[6] have found that ϕ_{ex} is not sensitive to large changes in a_f for the case without excluded volume. Numerical tests show that this is also true for the case with excluded volume. Therefore, by comparing steady-state fluorescencee yield data to ϕ_{ex} obtained from eq 18, the R_f value for solid solution is uniquely determined. The R_f obtained from the data presented in Figure 3 for solid solution is 13.1 Å.

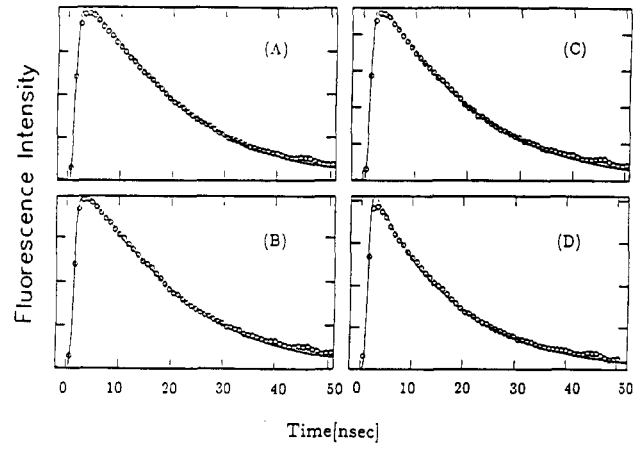

Figure 5. Time-resolved fluorescence data (circles) and theory (lines) for solid solutions with four concentrations. The concentrations for plots A–D are 0.105, 0.134, 0.224, and 0.470 M, respectively. The best fit is obtained with a_f = 0.22 Å and R_f = 13.1 Å.

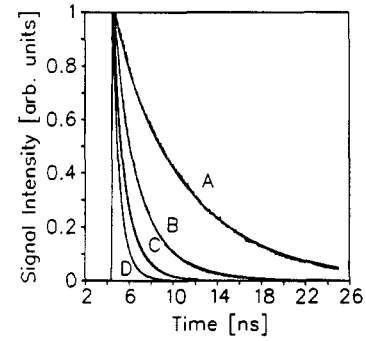

Figure 6. Time-resolved fluorescence data and theory for liquid solutions with four concentrations. The concentrations for plots A–D are 0.031, 0.11, 0.21, and 0.33 M, respectively. The best fit is obtained with a_f = 0.22 Å and R_f = 12.8 Å.

The liquid solution data in Figure 4 are given as a Stern–Volmer plot. In the limit that diffusion is infinitely fast this would be a straight line. In the limit that the reaction is diffusion limited, the initial slope is related to the rate parameters.[1,10,14] The samples studied here are between these two limits. Equation 18 was used to fit the data using eq 15 for the excited-state population. For each concentration, the measured diffusion constant (given above) was used. In Figure 4 the solid line is the best fit; the symbols are the data. The fit is sensitive to both parameters, and it is possible to obtain a well-defined unique fit. The parameters were found to be a_f = 0.22 Å and R_f = 12.8 Å.

Comparison of the yield plots for solid and liquid solutions shows the tremendous increase in electron transfer in the liquid solutions compared to the solid. For an acceptor concentration of 0.32 M, the relative fluorescence yield in the solid is ~25% while in the liquid it is ~1.6%.

B. Time-Resolved Fluorescence Data. The time-resolved fluorescence quenching data in SOA and DES are presented in Figures 5 and 6, respectively. The calculated excited-state population, $\langle P_{ex}(t) \rangle$, is convolved with the instrument response

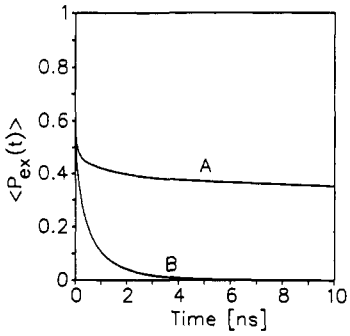

Figure 7. Calculation of the time dependence of donor quenching by electron transfer for the solid (curve A) and the liquid (curve B) solutions. The lifetime decay of the excited state is not included so that electron transfer can be compared more directly. The parameters are $C = 0.27$ M, $a_f = 0.22$ Å, $R_f = 13$ Å, and for the liquid solution, $D = 18.6$ Å^2/ns. Diffusion results in a large increase in electron transfer.

function and then compared to the data. The appropriate equation is

$$S(t) = \int_0^\infty \mathrm{IR}(t - t')\langle P_{ex}(t')\rangle \, dt' \qquad (19)$$

where IR(t) is the measured instrument response. For the solid solutions, only one parameter, a_f, was adjusted to fit the data. An $a_f = 0.22$ Å was obtained.

Figure 6 shows the dramatic change in the liquid data with DQ concentration. Both parameters a_f and R_f were adjusted to fit these liquid solution data. It is found that the best fits are obtained with $a_f = 0.22$ Å and $R_f = 12.8$ Å.

The solid and liquid solvents were chosen because they have very similar dielectric properties. Thus, a_f and R_f are expected to be similar for the same donor–acceptor pair even if the rate of diffusion differs greatly between the two systems. The fact that virtually identical electron-transfer parameters are obtained in liquid diethyl sebacate ($a_f = 0.22$ Å and $R_f = 12.8$ Å) and solid sucrose octaacetate ($a_f = 0.22$ Å and $R_f = 13.1$ Å) solutions demonstrates that the a_f and R_f parameters are not arbitrary fitting parameters. They are good molecular parameters capable of characterizing the forward photoinduced electron-transfer process. The consistency between the solid and liquid data and the quality of the fits to the liquid data also demonstrate that the statistical mechanical model does an excellent job of handling diffusion in the forward transfer component of the problem. There have been a number of theoretical treatments of the forward problem with diffusion.[10,11,12,38] The theory used here differs mildly by including acceptor–acceptor and donor–acceptor excluded volumes and a reflecting boundary condition.

Since electron transfer is extremely sensitive to distance, it is essential to know the initial conditions accurately. RU and DQ are both neutral. Therefore, initially the donors and acceptors are randomly distributed. In systems where both the donor and acceptor are ions,[13] it is difficult to determine the initial spatial configuration precisely. This could lead to difficulties in data fitting.

It can be seen by comparing Figures 5 and 6 that the excited-state population decays (electron transfer) are much faster in the liquid solution than in the solid solution. Figure 7 shows a calculation of the time-dependent donor quenching by electron transfer (excited-state lifetime decay not included) for the solid (A) and liquid (B) solutions. The parameters are those determined by experiment except that R_f has been rounded off to 13 Å for both the solid and the liquid. The difference is dramatic. At short time (<5 ps) the displacement of the molecules is negligible and the curves are identical. At longer time, diffusion in the liquid solution leads to more electron-transfer events and a faster depletion of the excited state. Diffusion of the molecules has a profound influence on the transfer process despite the fact that the transfer parameters, a_f and R_f, are virtually identical in the two systems. This can be understood qualitatively. In any electron-transfer system, the spatial separation across which electron transfer can occur is limited by the excited-state lifetime of the donor. In a solid, acceptors that are too far away from the excited donor to receive an electron within the donor lifetime do not participate in the transfer dynamics. In a liquid, acceptors which may have initially been too far from the donor can diffuse in at later times and receive an electron. This diffusive motion allows more acceptors to pass through the range of possible electron transfer in the liquid solution than exist near the donor in the immobile solid solution. The net result is that an increased rate of diffusion will increase the rate of depletion of the excited state by forward electron transfer.

C. Pump–Probe Data. In the simplest situation, the pump–probe observable is proportional to the population that is not in the ground state. This occurs if there is no stimulated emission or excited-state–excited-state (ES–ES) absorption. Thus, if the only absorbing state is the ground state, then the pump–probe observable is given by

$$S(t) = A[\langle P_{ex}(t)\rangle + \langle P_{re}(t)\rangle] \qquad (20)$$

where A is a constant determined by experimental parameters such as the laser intensity. Equation 20 comes from conservation of probability (see eq 17).

If the probe wavelength is in the spectral region of the fluorescence of the donor, stimulated emission will occur. This is the situation in these experiments. Because of stimulated emission, there is amplification of the probe intensity as it passes through the sample. This extra signal is proportional to the excited-state population and the stimulated emission cross-section. The contribution to the signal from removal of population from the ground state is proportional to the ground-state absorption coefficient (cross-section). The inclusion of stimulated emission in the analysis is accomplished by adding the ratio of the stimulated emission cross-section to the ground-state absorption cross-section to the coefficient in front of the excited-state population.[41] This gives

$$S(t) = A[(1.0 + \beta)\langle P_{ex}(t)\rangle + \langle P_{re}(t)\rangle] \qquad (21)$$

where β is the ratio of the stimulated emission cross-section to the absorption cross-section at the wavelength of interest.

In contrast to these amplifying effects, ES–ES absorption decreases the probe intensity. This effect can be included in the same manner as stimulated emission. The ratio of the absorption cross-section for the ES–ES absorption to the ground-state absorption cross-section is subtracted from the coefficient in front of the excited-state population. The observable is

$$S(t) = A[(1.0 + \beta - \gamma)\langle P_{ex}(t)\rangle + \langle P_{re}(t)\rangle] \qquad (22)$$

where γ is the ratio of the ES–ES absorption cross-section to the ground-state absorption cross-section.

In both SOA and DES at 532 nm, excited RU has a significant amount of stimulated emission and ES–ES absorption.[23] Although these two effects work in opposite directions on the signal, they do not completely cancel. The β's were measured in both SOA and DES at 532 nm. RU has mirror symmetry between the absorption and emission spectra, typical of this type of molecule.[24] Therefore, the absorption cross-section at the peak of the absorption spectrum will be equal to the stimulated emission cross-section at the peak of the fluorescence spectrum. The fluorescence cross-section at 532 nm is the ratio of the fluorescence intensity at 532 nm to that at the peak of the fluorescence multiplied by the peak absorption cross-section. The β's obtained from SOA and DES are 0.5 ± 0.1 and 0.3 ± 0.1, respectively. These values are similar to those measured by others.[23,25] The ES–ES cross-section is more difficult to measure because it overlaps with fluorescence and stimulated emission from the excited state and the absorption from the ground state. An early

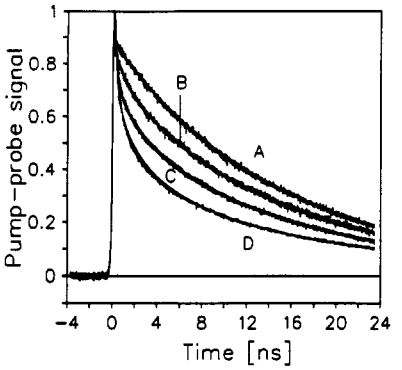

Figure 8. Pump–probe data for the solid solution. The curves labeled A–D have the following concentrations: 0, 0.051, 0.098, and 0.23 M, respectively. The peak at short time is due to a coherence artifact. The single set of electron-transfer parameters that fit all the data curves are R_b = 12.3 Å and a_b = 0.9 Å.

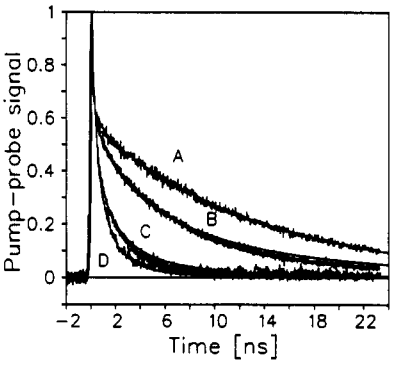

Figure 9. Pump–probe data for liquid solution. The curves labeled A–D have the following concentrations: 0, 0.04, 0.13, and 0.22 M. The peak at short time is due to a coherence artifact. The smooth lines are the fits using the back-transfer parameters obtained for solid solution, R_b = 12.3 Å and a_b = 0.9 Å. In these calculations the high-frequency value of the relative permittivity, ϵ_r = 2, was employed.

attempt[25] to measure the ES–ES absorption failed to find any at 532 nm. However, a more recent study[23] was able to detect the ES–ES absorption of RU at 532 nm. The data obtained from the study gave a $\gamma = 1 \pm 0.2$. The ions RU^+ and DQ^- do not absorb at 532 nm and are not included in the analysis.[26]

Since there is a significant uncertainty in the coefficient in front of the excited-state population ($B = 1 + \beta - \gamma$) in eq 22, the procedure used to fit the data involved adjustment of this coefficient within the error bars of β and γ. In the fitting procedure, a β was chosen and then the back electron-transfer parameters were fit. Then another β was chosen, and the back-transfer parameters were fit again.

For accurate comparison to the data, $S(t)$ needs to be convolved with the appropriate pulse shape functions of the pump and the probe. This is given by

$$I(t) = \int_{-\infty}^{\infty} G_{probe}(t - t') \int_{-\infty}^{t'} G_{pump}(t'') S(t' - t'')\, dt''\, dt' \quad (23)$$

where $G_{probe}(t')$ and $G_{pump}(t'')$ are Gaussians whose full width at half-maxima are given by the fwhm of the pulses, measured by autocorrelation.

Figure 8 displays pump–probe data taken on solid solutions for four acceptor concentrations. At short time the data are dominated by a coherence artifact. This is due to diffraction of the strong pump beam into the weak probe beam by a short-lived grating created when the pump and probe pulses directly overlap around $t = 0$. Measurements of the instrument response show that after 0.5 ns the data are not influenced by the coherence spike. For this reason, the data fitting was done at times greater than 0.5 ns. The fits yielded a unique set of back electron-transfer parameters: R_b = 12.3 Å and a_b = 0.9 Å. Spanning the region within the error bars of γ and β, the best fit was obtained with a $\gamma = 1.2$ and a $\beta = 0.4$. At any other values of γ and β, no choice of transfer parameters other than the unique set given above could reproduce the quality of the fit. Thus, the γ and β parameters do not degrade the reliability of the electron-transfer parameters.

In fitting the forward transfer data in the solid and liquid solutions, it was determined that the forward transfer parameters were virtually identical in the two media. In fact, if the solid transfer parameters had been used without modification, the agreement with the liquid data would be virtually the same as that displayed in Figure 6. The excellent agreement between theory and data shows that it is possible to handle the diffusion of the particles accurately. The processes for back-transfer in the solid and liquid are fundamentally different because of the Coulomb interaction between the ions. In the solid solution, the ions are immobile, so the fact that the particles are charged does not change the ability of the statistical mechanical theory to do the averaging over the nonrandom spatial distribution exactly.

In the liquid, it is necessary to account for not only diffusive motion, but also the nondiffusive motion caused by the attractive Coulomb interaction. This interaction is mediated by the dielectric properties of the solvent (see eq 16). In the theory, the dielectric properties come in through a single parameter, the relative permittivity.

The data for liquid solutions are presented in Figure 9. It shows the pump–probe observable for several concentrations. The spike around $t = 0$ is a coherence artifact. As the acceptor concentration is increased, the signal decays much faster. The signal depends on both the forward and back transfer rates. At higher concentration, the number of acceptors available for transfer is larger, and thus the rate of forward transfer is increased (Figure 6). This results in a greater number of ion pairs at any separation R. This in turn causes the back-transfer rate to also increase with higher concentration.

The solid lines shown in Figure 9 are calculations for the liquid pump–probe decay, using the back-transfer parameters measured in the solid solution (R_b = 12.3 Å and a_b = 0.9 Å). The ratios of the stimulated emission cross-section (β) and the ES–ES cross-section (γ) to the ground-state absorption cross-section were adjusted within their error bars to obtain the best fit. Like the solid solution, this improved the agreement between the data and the calculated curves. However, the back-transfer parameters that gave the best agreement with the data were again unchanged by varying γ and β. The values are $\beta = 0.4$ and $\gamma = 0.8$. The relative permittivity used in the calculation is $\epsilon_r = 2$. This is the high-frequency value.[42] As can be seen from the figure, the agreement between theory and experiment is very good. This is particularly true considering the fact that there are no adjustable parameters in the calculation. The forward transfer parameters were obtained from the fluorescence measurements, and the back-transfer parameters are those measured from the solid solution. However, the high-frequency relative permittivity was employed. As discussed below, it is not clear that this is the proper choice.

Figure 10 again shows the data but with calculations using the low-frequency relative permittivity,[42] $\epsilon_r = 5$; all other parameters are identical. The agreement between the data and the calculations is poor. Extensive fitting of the data using the low-frequency relative permittivity was performed. R_b and a_b were varied together and independently over an extremely wide range, including values that are unphysical. The agreement could not be improved and become increasingly worse as the parameters were adjusted away from the values measured in solid solution. The calculated curves have fundamentally the wrong shape. Clearly the use of the low-frequency relative permittivity underestimates the strength of the Coulomb interaction. When the high-frequency relative permittivity is used, the calculated curves have essentially the correct functional form and are able

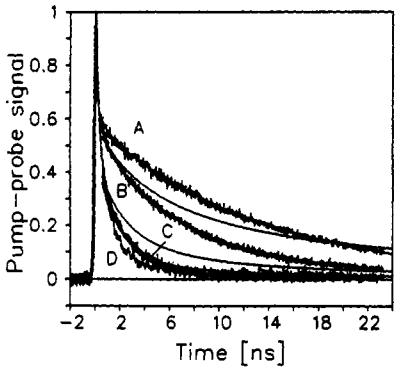

Figure 10. Pump–probe data for liquid solutions. This is the same data as those displayed in Figure 9. The calculations are also identical, R_b = 12.3 Å and a_b = 0.9 Å, with the exception that the low-frequency relative permittivity was employed, i.e., ϵ_r = 5. The agreement is poor and cannot be improved by varying the back-transfer parameters.

to reproduce the concentration dependence observed in the data. This suggests that the use of the high-frequency relative permittivity is appropriate. Intermediate values of the relative permittivity were also used, and it was found that the data were more closely fitted by the calculated curves as the high-frequency value was approached.

The relative permittivity has two contributions. The first is a local effect, and occurs on a time scale much shorter than the electron-transfer events being observed in these experiments. The incident electric field of the laser pulse causes ultrafast polarization of the solvent electrons, as well as certain restricted motions of molecular substituents. Effects on this time scale are manifested by a change in the optical index of refraction. In this regime, the high-frequency relative permittivity is equal to the square root of the optical refractive index. The second contribution to the relative permittivity involves reorientation of the solvent molecules to align their dipoles with the fields generated by the sudden formation of the ions. For an electric field applied to bulk DES, this will occur with the rate of orientational relaxation of the solvent molecules. The orientational relaxation time, τ_r, was calculated approximately by making a molecular model, determining its volume, V, and using the Debye–Stokes–Einstein equation

$$\tau_r = V\eta/KT \tag{24}$$

where η is the viscosity and T is the absolute temperature in kelvin. DES can assume a wide variety of conformations. The various conformations have different volumes, and therefore different τ_r's. From the model, the volume of various conformations was determined. The slowest τ_r is 600 ps, while the fastest is 150 ps. Typical values are in the range of 400–500 ps.

The pump–probe data shown in Figure 9 decay more slowly than τ_r, particularly at low acceptor concentration. However, the long decays are in part due to the rate of forward transfer. The correct comparison of time scales is between τ_r and the lifetime of ion pairs once they are created. This can be done by calculating the average survival time using the excited-state (eq 6) and reactive-state (eq 9) survival probabilities. The average survival time is obtained by calculating the probability that the ions exist at time t after they are formed:

$$\langle P(t)\rangle = \frac{\int_{R_m}^{\infty} S_{re}(R|t)\, 4\pi C k_f(R) \int_0^{\infty} S_{ex}(R|t')\langle P_{ex}(t')\rangle\, dt' R^2\, dR}{\int_{R_m}^{\infty} 4\pi C k_f(R) \int_0^{\infty} S_{ex}(R|t')\langle P_{ex}(t')\rangle\, dt' R^2\, dR} \tag{25}$$

The characteristic lifetime of this probability decay curve can be defined as the time at which the curve has fallen to e^{-1} times its original value. This lifetime is taken to be the average survival time of the reactive-state pairs. Given that a reactive-state pair is formed at time t = 0, this value is the average length of time which this pair lives before geminately recombining. The value obtained from the calculation of $\langle P(t)\rangle$ is approximately 500 ps. This value is somewhat skewed to long time due to the small fraction of ions which escape recombination. This escape acts to increase the survival probability, thus increasing the lifetime of $\langle P(t)\rangle$.

The agreement between the data and calculations using the high-frequency relative permittivity and *no adjustable parameters* indicates that additional aspects of the overall system should be taken into account. The orientational relaxation time, τ_r, that was calculated is for DES as a bulk liquid. However, the orientational relaxation time of interest is actually that of DES in close proximity to the RU cation and the DQ anion. These molecular ions will make a significant perturbation of the local DES liquid structure. An increase in τ_r locally would make the pertinent dielectric properties correlate to the high-frequency regime. Another consideration is the distance scale associated with the ion pair Coulomb interaction. Typical distances for the initial ion pair separations are 12–13 Å center-to-center. This is only 3–4 Å edge-to-edge. Although the electric field is not strictly directed along the line connecting the molecular centers, it should be noted that there are very few solvent molecules participating in screening the Coulomb interaction. There will only be one or two solvent molecules between the ions. In contrast, the relative permittivity is a bulk property. For the short distances that are important in electron transfer, the molecularity of the solvent can be important.[27] These factors indicate that the low-frequency relative permittivity is not appropriate. However, this is a significant point that requires detailed study.

The forward and back electron-transfer parameters obtained by fitting the data yield theoretical curves that are consistent with the experimental results in both solid and liquid solutions, over a range of concentrations. This demonstrates the ability of the statistical mechanical model to handle the influence of diffusion on electron transfer. Accurate analysis of back-transfer, which involves diffusion modified by the Coulomb interaction with nonrandom initial conditions, is significant. The theory can incorporate any form of the distance dependence of the transfer rate. The exponential form employed here provides a consistent description of the experimental data. However, the very shortest range transfer events, which occur faster than the experimental time scale (50–100 ps), are not probed. Future studies will examine these issues in more detail.

Acknowledgment. The authors would like to thank Professor Masanori Tachiya for valuable discussions about ion survival time calculations. This work was supported by the Department of Energy, Office of Basic Energy Sciences (Grant DE-FG03-84ER13251). We would also like to thank the Stanford Center for Materials Research for use of the time-correlated single photon counting instrument and acknowledge an NSF departmental instrumentation grant (No. CHE 88-21737) which provided computer equipment used in the calculations. K.W. was supported by an NSF predoctoral fellowship.

References and Notes

(1) Guarr, T.; McLendon, G. *Coord. Chem. Rev.* **1985**, *68*, 1.
(2) Devault, D. Q. *Rev. Biophys.* **1980**, *13*, 387.
(3) Popovic, Z. D.; Kovacs, G. J.; Vincett, P. S. *Chem. Phys. Lett.* **1985**, *116*, 405.
(4) Dorfman, R. C.; Fayer, M. D. *J. Chem. Phys.*, in press.
(5) Lin, Y.; Dorfman, R. C.; Fayer, M. D. *J. Chem. Phys.* **1989**, *90*, 159.
(6) Inokuti, M.; Hirayama, F. *J. Chem. Phys.* **1965**, *43*, 1978.
(7) Tachiya, M.; Mozumder, A. *Chem. Phys. Lett.* **1974**, *28*, 87.
(8) Song, L.; Dorfman, R. C.; Swallen, S. F.; Fayer, M. D. *J. Phys. Chem.* **1991**, *95*, 3454.
(9) Najbar, J. *J. Chem. Phys.* **1988**, *120*, 367.
(10) Rice, S. A. *Diffusion-Limited Reactions*; Elsevier: Amsterdam, 1985.

(11) Tachiya, M. *Radiat. Phys. Chem.* **1983**, *21*, 167.
(12) Sano, H.; Tachiya, M. *J. Phys. Chem.* **1979**, *71*, 1276.
(13) Eads, D. D.; Dismer, B. G.; Fleming, G. R. *J. Chem. Phys.* **1990**, *93*, 1136.
(14) Birks, J. B. *Photophysics of Aromatic Molecules*; Wiley-Interscience: London, 1970.
(15) Agmon, N.; Szabo, A. *J. Am. Chem. Phys.* **1990**, *92*, 5270.
(16) Rabinovich, S.; Agmon, N. *Chem. Phys.* **1990**, *48*, 11.
(17) Agmon, N. *J. Chem. Phys.* **1989**, *90*, 3765.
(18) Blumen, A.; Manz, J. *J. Chem. Phys.* **1979**, *71*, 4694.
(19) Blumen, A. *J. Chem. Phys.* **1980**, *72*, 1632.
(20) Stein, A.; Peterson, K. A.; Fayer, M. D. *J. Chem. Phys.* **1990**, *92*, 5622.
(21) Kennard, O.; Watson, D. G.; Rodgers, J. R. *Crystal Data Determinative Tables*, 3rd ed.; U.S. Department of Commerce, National Bureau of Standards, and the JCPDS-International Center for Diffraction Data: Washington, DC, 1978.
(22) Shoemaker, D. P.; Garland, C. W.; Steinfeld, J. I.; Nibler, J. W. *Experiments in Physical Chemistry*, 4th ed.; McGraw-Hill Book Co.: New York, 1981.
(23) Lohmannsroben, H. G. *Appl. Phys. B* **1988**, *47*, 195.
(24) Berlman, I. B. *Handbook of Fluorescence Spectra of Aromatic Molecules*; Academic Press: New York, 1971.
(25) Yee, W. A.; Kuzmin, V. A.; Kliger, D. S.; Hammond, G. S.; Twarowski, A. J. *J. Am. Chem. Soc.* **1979**, *101*, 5104.
(26) Shida, T. *Electronic Absorption Spectra of Radical Ions*; Elsevier: Amsterdam, 1988.
(27) Morita, T.; Ladanyi, B. M.; Hynes, J. T. *J. Phys. Chem.* **1979**, *93*, 1386.
(28) Closs, G. L.; Miller, J. R. *Science* **1988**, *240*, 440.
(29) Agrest, M. M.; Kilin, S. F.; Rikenglaz, M. M.; Rozman, I. M. *Opt. Spectrosc.* **1969**, *27*, 514.
(30) Kusba, J.; Sipp, B. *Chem. Phys.* **1988**, *124*, 223.
(31) Sipp, B.; Voltz, R. *J. Chem. Phys.* **1983**, *79*, 434.
(32) Sipp, B.; Voltz, R. *J. Chem. Phys.* **1985**, *83*, 157.
(33) Steinberg, I. Z.; Katchalski, E. *J. Chem. Phys.* **1968**, *48*, 2404.
(34) Yokota, K.; Tanimoto, O. *J. Phys. Soc. Jpn.* **1967**, *22*, 779.
(35) Allinger, K.; Blumen, A. *J. Chem. Phys.* **1980**, *72*, 4608.
(36) Allinger, K.; Blumen, A. *J. Chem. Phys.* **1981**, *75*, 2762.
(37) Baumann, J.; Fayer, M. D. *J. Chem. Phys.* **1986**, *85*, 4087.
(38) Dorfman, R. C.; Lin, Y.; Fayer, M. D. *J. Phys. Chem.* **1989**, *93*, 6388.
(39) Dorfman, R. C.; Tachyia, M.; Fayer, M. D. *Chem. Phys. Lett.* **1991**, *179*, 152.
(40) Vermeglio, A. *Function of Quinones in Energy Conserving Systems*; Academic Press: New York, 1982.
(41) Song, L.; Fayer, M. D. *J. Lumin.* **1990**, *50*, 75.
(42) The high-frequency dielectric constant of DES was obtained by calculating the square of the high-frequency index of refraction. The index of refraction was obtained from the Aldrich Chemicals catalog as well as measured using an Abeé refractometer. The two values agreed to within error. The low-frequency dielectric constant was measured using a capacitance bridge at 1 kHz and 120 Hz. It was found to be constant within this range, and to be independent of acceptor (DQ) concentration.
(43) Dorfman, R. C.; Lin, Y.; Fayer, M. D. *J. Phys. Chem.* **1990**, *94*, 8007.
(44) Chandrasekhar, S. *Rev. Mod. Phys.* **1943**, *15*, 1.
(45) Tachiya, M. *J. Chem. Soc., faraday Trans. 2* **1979**, *75*, 271.
(46) Mikhelashvili, M. S.; Feitelson, J.; Dodu, M. *Chem. Phys. Lett.* **1990**, *171*, 575.
(47) Schulten, Z.; Schulten, K. *J. Chem. Phys.* **1977**, *66*, 4616.
(48) Werner, H. J.; Schulten, Z.; Schulten, K. *J. Chem. Phys.* **1977**, *67*, 646.